Descriptor and scaling relations for ion mobility in crystalline solids

Mohsen Sotoudeh[*,†] and Axel Groß[*,†,‡]

†*Institute of Theoretical Chemistry, Ulm University, Albert-Einstein-Allee 11, 89081 Ulm, Germany*

‡*Helmholtz Institute Ulm (HIU) for Electrochemical Energy Storage, Helmholtzstraße 11, 89069 Ulm, Germany*

E-mail: mohsen.sotoudeh@uni-ulm.de; axel.gross@uni-ulm.de

Abstract

Ion mobility is a critical performance parameter in electrochemical energy storage and conversion, but also in other electrochemical devices. Based on first-principles electronic structure calculations, we have derived a descriptor for the ion mobility in battery electrodes and solid electrolytes. This descriptor is entirely composed of observables that are easily accessible: ionic radii, oxidation states and the Pauling electronegativities of the involved species. Within a particular class of materials, the migration barriers are connected to this descriptor through linear scaling relations upon the variation of either the cation chemistry of the charge carriers or the anion chemistry of the host lattice. The validity of these scaling relations indicates that a purely ionic view falls short of capturing all factors influencing ion mobility in solids. The identification of these scaling relations has the potential to significantly accelerate the discovery of materials with desired mobility properties.

Introduction

Electrochemical energy storage devices play a central role in our attempts towards decarbonization through the storage of volatile renewable energy and the emission-free usage of vehicles and mobile devices. Significant progress has been made in this respect due to the development of advanced Li-ion battery technologies.[1,2] In addition, recently so-called post Li-ion technologies[3,4] have drawn a lot of attention in order to address, among others, sustainability issues associated with the materials typically used in Li-ion batteries.[5,6] In post-Li ion batteries, other charge carriers such as monovalent Na and K cations[7,8] or divalent Mg and Ca cations[9–13] are used. These post-Li-ion batteries, in particular those based on multivalent ions, can compete with existing Li-ion batteries or even outperform them, as far as energy density and safety are concerned,[14,15] the latter in particular with respect to their lower tendency for dendrite growth.[16–20] Furthermore, as liquid electrolytes are prone to corrosion processes and often represent fire hazards because of their flammability, all solid-state

batteries with higher safety and better electrochemical stability[21] based on materials such as inorganic oxides,[22,23] hydrides,[24–26] and chalcogenides[27,28] have been intensively studied for all possible charge carriers.

A critical parameter that significantly influences the performance of batteries is the ion mobility both in the electrolyte and in the electrodes.[29–31] In particular batteries based on multivalent ions such as Mg^{2+} are plagued with low ion mobility[32–34] due to their stronger interaction with the host structures compared to monovalent ions such as Li^{+}. Hence the identification and development of materials with improved ion mobility are essential for more efficient electrochemical energy storage devices. However, ion conduction in solids is not only important in battery materials but also in many other applications such as, e.g., solar cells.[35]

A very useful concept in order to accelerate materials discovery is based on so-called descriptors.[36,37] They represent fundamental materials properties or combinations thereof that are correlated with a desired or undesired functionality of the material. This concept has been very successfully used in heterogeneous catalysis,[38] in particular in connection with so-called scaling relations,[39] but also already in battery research.[20] The identification of descriptors can significantly speed up the search for new materials with desired functional properties because once they are identified only the particular descriptors need to be optimized in a first step. Thus promising candidate materials can be proposed whose properties can then be scrutinized in detail.

In fact, also with respect to ion mobility in solids a number of possible descriptors have been proposed, based on, e.g., the lattice volume and ionic size,[28,29] the choice of the anion sublattice,[29,40] the lattice dynamics,[29,41,42] or the preferred crystal insertion site.[30] However, many of the identified descriptors are restricted to some particular crystal structure. Furthermore, some are based on materials properties that are not easily accessible. Hence it is fair to say that so far no convenient descriptor has been established that is able to predict ion mobility across a set of different structures.

Based on the results of first-principles density functional theory (DFT) calculations and

physico-chemical reasoning, here we propose such a *c*onvenient descriptor for the ion mobility, the so-called migration parameter or number, that is based on the product of Pauling's electronegativity, ionic radii and oxidation states of the involved compounds, all properties that are easily accessible for any material. This particular descriptor, whose choice is also supported by a statistical analysis of our first-principles results, goes beyond current proposals by considering also deviations from a purely ionic interaction between the migrating ion and the host lattice. According to our calculations, the activation barrier for migration is connected to this migration number via linear scaling relations within particular materials classes. This allows to predict the activation barriers both for the variation of the cation chemistry of the migrating ion as well as for the variation of the anion chemistry of the host lattice. Thus this descriptor will most probably significantly accelerate the discovery of materials with favorable mobility properties. As this migration number is based on basic physico-chemical quantities, it also enables a deeper fundamental understanding of the principles underlying ion mobility.

Results and Discussion

From a microscopic viewpoint, migration or diffusion in solid crystalline materials occurs by atomic hops in a lattice. Such jump processes are typically thermally activated, and the corresponding tracer diffusion coefficient is given by

$$D^{\mathrm{tr}} = D_0^{\mathrm{tr}} \exp\left(-\frac{E_a}{k_{\mathrm{B}}T}\right) \ . \tag{1}$$

Here D_0^{tr} is the pre-exponential factor, k_B the Boltzmann constant, and T the absolute temperature. E_a is the activation barrier corresponding to the energy barrier along the minimum energy path connecting two equivalent intercalation sites, as illustrated in Fig. 1. Such an minimum energy path can be determined by automatic search routines.[43] In the present work, we have used the nudged elastic band method (NEB)[44] in the DFT calcu-

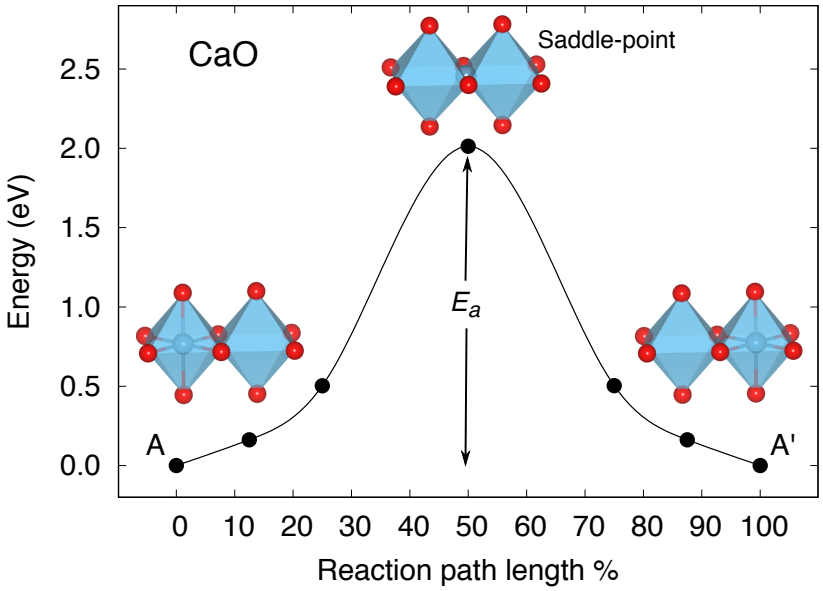

Figure 1: Illustration of a cation interstitial migration mechanism, using Ca diffusion in CaO as an example. A diffusion event corresponds to the migration of the Ca cation from the energetically most favorable octahedral site A to the nearest equivalent site A′ through the transition state which corresponds to a saddle-point in the multi-dimensional potential energy surface and which can be derived by first-principles electronic structure calculations. The activation energy or diffusion barrier is denoted by E_a which corresponds to the energy difference between the saddle-point and the initial configuration.

lations to derive the activation barrier E_a. The electronic structure calculations were performed using the Vienna *Ab-initio* Simulation Package (VASP) [45] employing the Projector Augmented Wave (PAW) [46] method with the exchange-correlation effects being described with the Perdew-Burke-Ernzerhof (PBE) functional. [47] Further details are provided in the Supporting Information.

Motivated by the goal to identify the fundamental factors determining ion mobility in solids, in a previous study [28] we had derived the activation barriers for diffusion of a number of ions of varying size and charge in the same host lattice, a chalcogenide spinel. We obtained the expected results, namely that the size and the charge of the diffusing ion matter. However, the ionic radius of the charge carrier alone could not explain the observed trends, but rather the distance between the ion in the tetrahedral site and the nearest chalcogenide atom. In order to further elucidate the mobility-determining factors, we decided to look at structurally simpler compounds, namely binary A_nX_m materials with A being the migrating

ion. In total, we looked at 35 different compounds with Li, Mg, and Ca as the migrating ion A.

For these binary materials, we again found that size and charge of the propagating ions matter, but not in a very systematic way, as already observed by others.[29] However, we could recently show that the stability of ions in chalcogenide spinels can only be understood if deviations from a purely ionic interaction are taken into account.[48] It is essential to realize that the considered binary materials span the whole range of interaction characteristics between metallic and ionic bonding. Such bonding characteristics can in fact been classified in so-called Van Arkel-Ketelaar triangles[49] in which compounds are placed according to the mean electronegativity χ_{mean} (x-axis) and the electronegativity difference $\Delta\chi$ (y-axis) of the constituting elements.

Fig. 2a shows the Van Arkel-Ketelaar triangle including the Mg binary compounds considered in this study. A large difference in electronegativity indicates ionic bonding characteristics (shown in yellow), as present in MgO and MgF_2. CsF (not shown) would lie at the apex of the triangle. At the bottom of the triangle corresponding to a vanishing electronegativity difference, an increasing mean electronegativity is associated with more directional bonding. Hence the lower right corner gathers covalent systems whereas the lower left corner contains metallic systems.

The Mg_nX_m binaries considered in this study all fall along a line between metallic and ionic bonding which is based on the fact that the cation in the binaries, Mg^{2+}, has not been varied. In detail, MgF_2 has the highest electronegativity difference $\Delta\chi$ indicating a strong ionic bond. This is also true for MgO, whereas Mg_2Si is associated with the lowest value $\Delta\chi$ demonstrating metallic bonding. The remaining compounds, Mg-halides, Mg-chalcogenides, Mg-pnictides, and Mg-tetrels, are located between strong ionic and metallic bonding indicated by the green area. They are divided into three groups. $MgCl_2$, $MgBr_2$, and Mg_3N_2 are characterized by a large electronegativity difference of about 1.7 demonstrating a predominately ionic bonding (light yellow region). MgI_2, MgS, and MgSe have $\Delta\chi \approx 1.3$,

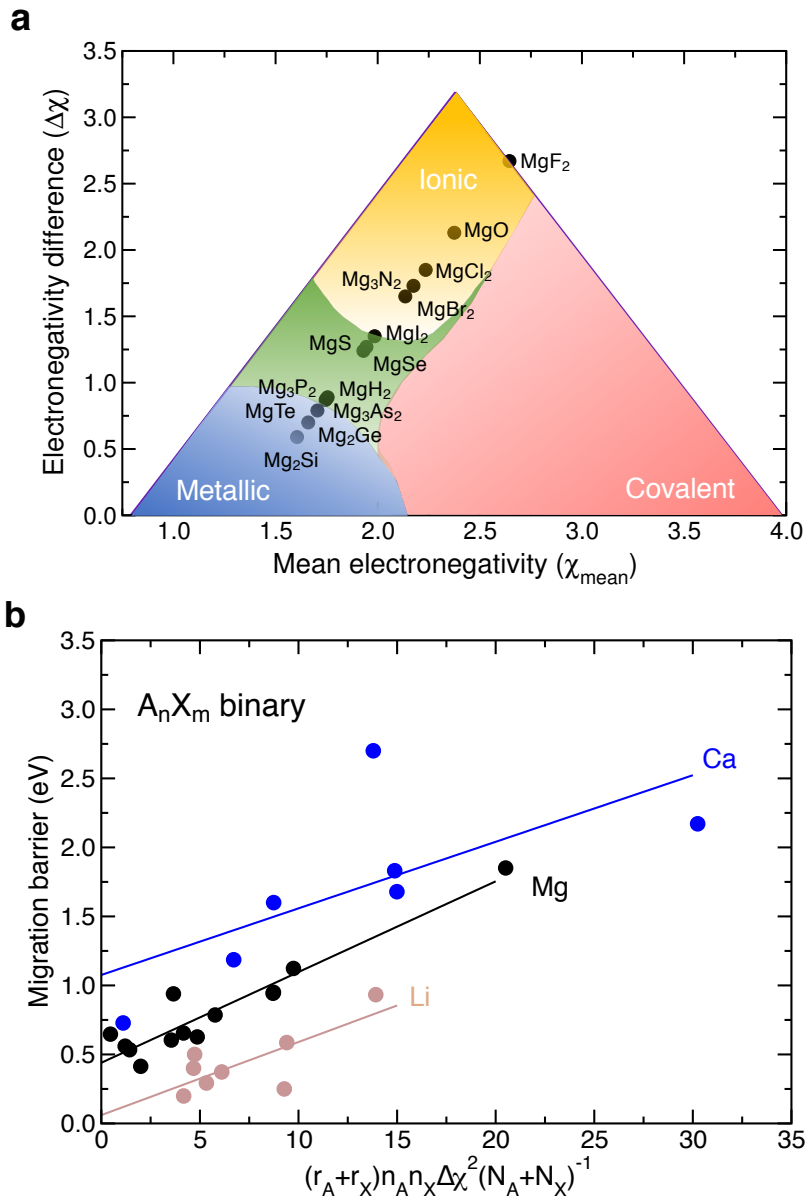

Figure 2: A_nX_m binaries considered in this study. (a) Van Arkel-Ketelaar triangle with the considered Mg_nX_m binaries plotted as a function of the mean electronegativity and the difference in the electronegativity of the two components. (b) Calculated activation energies for the migration of A = Li, Mg, and Ca in A_nX_m binaries as a function of the migration number $N_{\mathrm{migr}}^{\mathrm{AX}}$ for various elements X according to Eq. (2). The solid lines correspond to linear regressions of these results.

the other Mg binaries have electronegativity differences below 1.

The fact that also non-ionic components of the interaction contribute to the bonding in nominally ionic crystals[48] suggests that also the interaction characteristics within the

considered compounds represented by the electronegativity difference $\Delta\chi^2$ influences the ion mobility. Together with the well-known dependence of the diffusion barriers on the ionic radii (r_i) and oxidation states (n_i) of the involved compounds, this observation motivated us to define the *migration* parameter or number N_{migr}

$$N_{\mathrm{migr}}^{\mathrm{AX}} = (r_{\mathrm{A}} + r_{\mathrm{X}}) n_{\mathrm{A}} n_{\mathrm{X}} \Delta\chi_{\mathrm{AX}}^2 / (N_{\mathrm{A}} + N_{\mathrm{X}}) \tag{2}$$

as the product of these three quantities where the ionic radii r_{A} and r_{X} are given in Å, and n_{A} and n_{X} are the absolute values of the formal integer oxidation states or numbers. In addition, also the number of atoms of the corresponding species in the unit cell of the crystal N_{A} and N_{X} enters. In Fig. 2b, we plot the dependence of the migration barriers as a function of the migration parameter for the three migrating ions Li, Mg and Ca in the low vacancy limit. In spite of some outliers, overall the migration barriers nicely follow separate scaling relations for each migrating ion

$$E_a^{\mathrm{A}}(\mathrm{X}) = E_0^{\mathrm{A}} + C^{\mathrm{A}}(r_{\mathrm{A}} + r_{\mathrm{X}}) n_{\mathrm{A}} n_{\mathrm{X}} \Delta\chi_{\mathrm{AX}}^2 / (N_{\mathrm{A}} + N_{\mathrm{X}}) = E_0^{\mathrm{A}} + C^{\mathrm{A}} N_{\mathrm{migr}}^{\mathrm{AX}} \, . \tag{3}$$

These presence of universal scaling relations strongly suggest that the same factors govern the ion mobility in all considered binary compounds. It is no surprise that there are a few outliers indicating that other critical contributions to the activation energies can play a role, for example Coulomb interactions beyond those represented by the oxidation states, quantum mechanical overlap effects and polarization.[29]

In order to verify that we identified the crucial parameters governing ion mobility in these binary materials, we applied a statistical compressed-sensing approach using the sure-independence screening and sparsifying operator SISSO,[50] as described in detail in the Supporting Information, to search for possible descriptors. We used the following input parameters or so-called primary features: number of atoms in the unit-cell (N_{atom}) and the atomic masses of the two elements in the binary compound (m_{A}, m_{X}), their formal oxidation

numbers (n_{A}, n_{X}) and ionic radii (r_{A}, r_{X}), the Pauling electronegativity (χ_{A}, χ_{X}) of both elements, the A-X bond distances $d_{\mathrm{A-X}}$, and the unit cell volume V. This approach allows to vary the dimensionality Ω of the descriptor space, and the descriptor is expressed as a linear combination of so-called features that are non-linear functions of the input parameter or primary features. For $\Omega = 1$, we obtained the descriptor

$$d = (((n_{\mathrm{X}}/n_{\mathrm{A}}) - \cos(n_{\mathrm{X}}))/((\chi_{\mathrm{X}})^6 \cdot \sin(m_{\mathrm{X}}))) \ , \tag{4}$$

whereas for $\Omega = 2$ we found a two-dimensional descriptor consisting of the two features d_1 and $\mathrm{d_2}$:

$$d_1 = (n_{\mathrm{X}})^2 \times (r_{\mathrm{Mg}} + r_{\mathrm{X}}) \ , \tag{5}$$

$$d_2 = (\chi_{\mathrm{X}})^3/(N_{\mathrm{atom}}) \ . \tag{6}$$

Indeed these findings confirm that the oxidation states reflecting the charge of the atoms, the ion radii and the electronegativity differences are the determining factors for the migration barriers. Interestingly, the unit cell volume V which has been shown to substantially influence the ionic mobility in some structural families[28,29] does not show up in these statistically derived descriptors. However, note that the functional dependencies found by the SISSO operators do not allow for a straightforward interpretation of the physico-chemical factors underlying the migration process.

Therefore we decided to look for a verification whether the observed scaling relations as a function of the migration parameter (Eq. (2)) are also valid for other material types. As this study was originally motivated by the results for migration barriers of A^{n+} in $\mathrm{AB_2X_4}$ spinel structures, we reconsidered our previous results.[28] For these structures, the NEB method was again applied in the low vacancy limit. In Fig. 3, we have plotted the migration barriers E_a(in eV) as a function of the migration parameter Eq. (2) for $\mathrm{ASc_2S_4}$ and $\mathrm{MgSc_2X_4}$ spinels (panel a) and $\mathrm{ACr_2S_4}$ and $\mathrm{MgCr_2X_4}$ spinels (panel b), respectively. Note that the factor

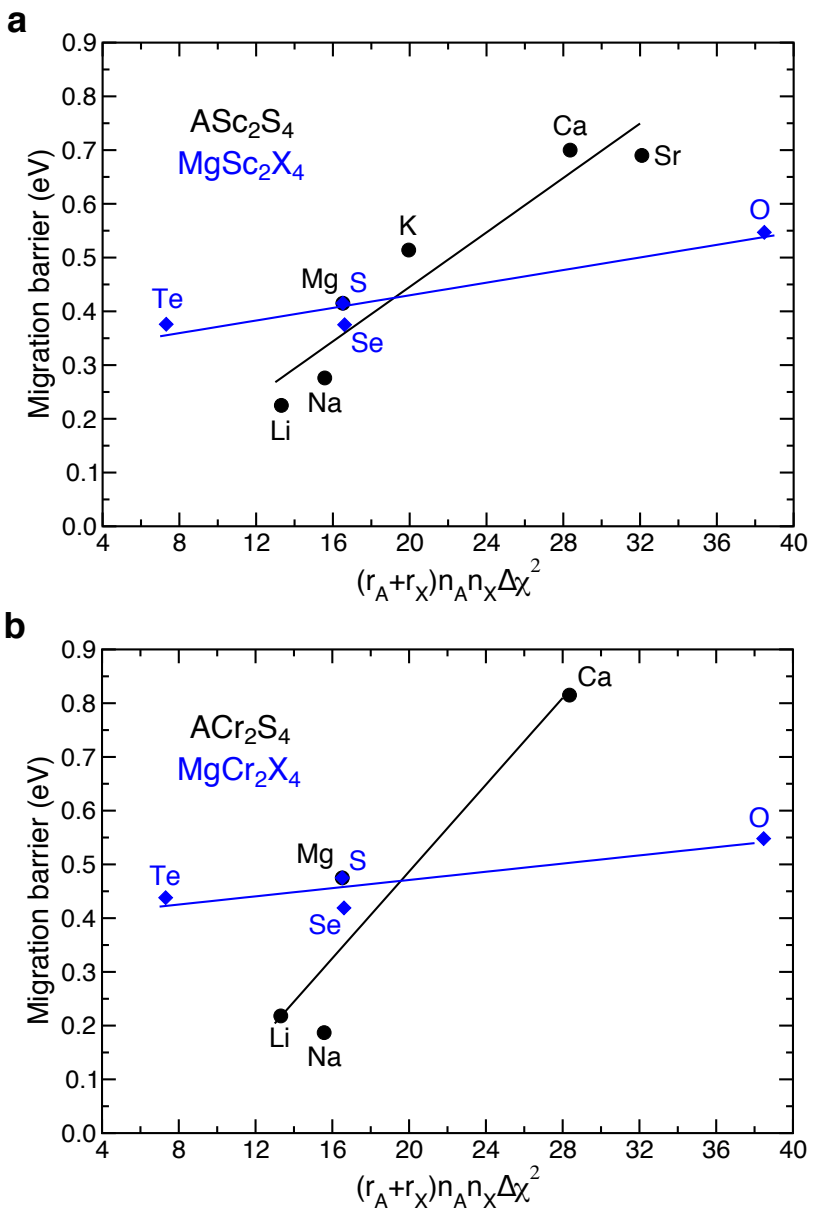

Figure 3: Panel a: migration barriers (in eV) in ASc_2X_4 as a function of the migration parameter $(r_A + r_X)n_A n_X \Delta\chi^2_{AX}$ (Eq. (2)) for ASc_2S_4 (black symbols) and $MgSc_2X_4$ spinels (blue symbols) for various mono- and multivalent cations A^{n+} and anions X^{n-}. Panel b: the same as in panel a, but with Sc replaced by Cr.

$1/(N_A + N_X)$ has been omitted in the definition of the x-axis as this factor is constant for all considered materials. Again, as in Fig. 2, we find a linear scaling of the migration barriers upon variation of the anions X^{n-} (blue symbols). Interestingly enough, we also find additional scaling relations upon variation of the cations Li^+, Na^+, K^+, Mg^{2+}, Ca^{2+}, and Sr^{2+} (black symbols) (note that the $MgSc_2S_4$ and $MgCr_2S_4$ spinels, respectively, are part of

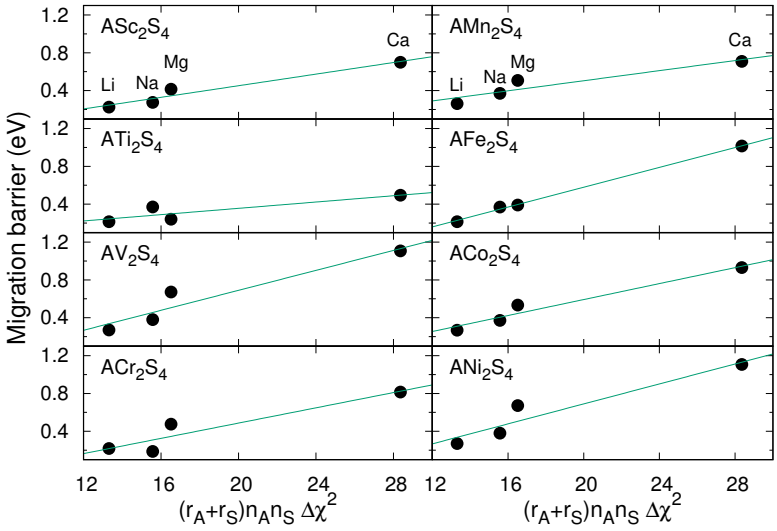

Figure 4: Migration barriers (in eV) in AB_2S_4 spinels as a function of the migration number $N_{\mathrm{migr}}^{\mathrm{AS}}$ for eight different transition metal cations B= Sc, Ti, V, Cr, Mn, Fe, Ci and Ni upon variation of migrating cations A= Mg, Na, K, Mg, and Ca.

both corresponding subsets). These results demonstrate that the scaling relations Eq. (3) are independently valid for the variation of either the cation chemistry of the migrating ions A^{n+} or the variation of the anion chemistry of the host lattice ions X^{n-}.

As Fig. 3 illustrates, upon variation of the host lattice cations B^{n+} present in the sulfide spinels AB_2X_4, which are typically transition metal cations, the slope of the linear scaling relations represented by the parameter C^{A} in Eq. 2 changes. We have determined the height of the migration barriers for the six additional transition metals B= Ti, V, Mn, Fe, Co and Ni as a function of the migration number upon variation of the migrating cations A^{n+} and collected the results in Fig. 4. We again find that the migration barriers follow linear scaling

Table 1: Difference $\Delta E_a^{\mathrm{A}}(\mathrm{B})$ in eV between the lowest and the highest migration barrier for the charge carriers A = Li, Na, K, Mg and Na in AB_2X_4 spinels upon variation of the eight considered transition metals B shown in Fig. 4.

Migrating ion	Li^+	Na^+	K^+	Mg^{2+}	Ca^{2+}
$\Delta E_a^{\mathrm{A}}(\mathrm{B})$ (eV)	0.08	0.19	0.42	0.44	0.61

relations, but with different slopes. It is interesting to note that the difference $\Delta E_a^{\mathrm{A}}(\mathrm{B})$ between the lowest and the highest migration barrier upon variation of the eight considered transition metals B increase with the size and the charge of the migrating cations A^{n+}, as illustrated in Tab. 1. Apparently for increasing charge and size of the host lattice cations B, the specific nature of the interaction between the cations A and B becomes more prominent, as far as the migration barriers for A are concerned.

Note that in the migration number $N_{\mathrm{migr}}^{\mathrm{AX}}$ (Eq. 5), parameters of the migrating cations A and of the anions X of the host lattice enter. However, in the spinels $\mathrm{AB_2X_4}$ there are also further cations B^{n+}, typically transition metal cations, present that are not considered in the migration number, but which should also be of significance in the A-ion transport. In these materials, the B-X bond is dominantly covalent. In Fig. 5, we have plotted migration barriers for $\mathrm{MgB_2X_4}$ spinels as a function of the squared electronegativity difference between transition metal B and anion X (panel a) and the ionic radius of the transition metal B (panel b) for a number of $\mathrm{MgB_2X_4}$ spinels. Note that there is some scatter in the data. However, there is a clear minimum in the height of the migration barriers in panel 5a for values of $\Delta\chi^2 \approx 2$. Furthermore, the unit-cell volume of the spinel increases by substituting a larger B cation into the structure. Again we find a clear minimum in the height of the migration barriers in panel 5b, here for the ionic radius of the transition metal B at values of $r_{\mathrm{B}} \approx 1.1$. These findings reflect that also the choice of the B cations play a role in minimizing the ion migration barriers in the spinel compounds. However, we did not manage to identify any linear scaling relations upon the variation of the cation B. Based on the identification of these pronounced minima and the corresponding matching properties of Zr, we identified $\mathrm{MgZr_2S_4}$ as a promising ion conductor with a high ion mobility, and indeed we found that $\mathrm{MgZr_2S_4}$ has a rather low Mg migration barrier of only 0.3 eV.

We have applied the concept to yet another class of materials that are widely used as battery materials, namely olivines.[51] Figure 6 shows the migration barriers in the olivine $\mathrm{AFeSiO_4}$ as a function of the migration parameter $(r_{\mathrm{A}} + r_{\mathrm{O}}) n_{\mathrm{A}} n_{\mathrm{X}} \Delta\chi^2_{\mathrm{AO}}$ (Eq. (2)) for varying

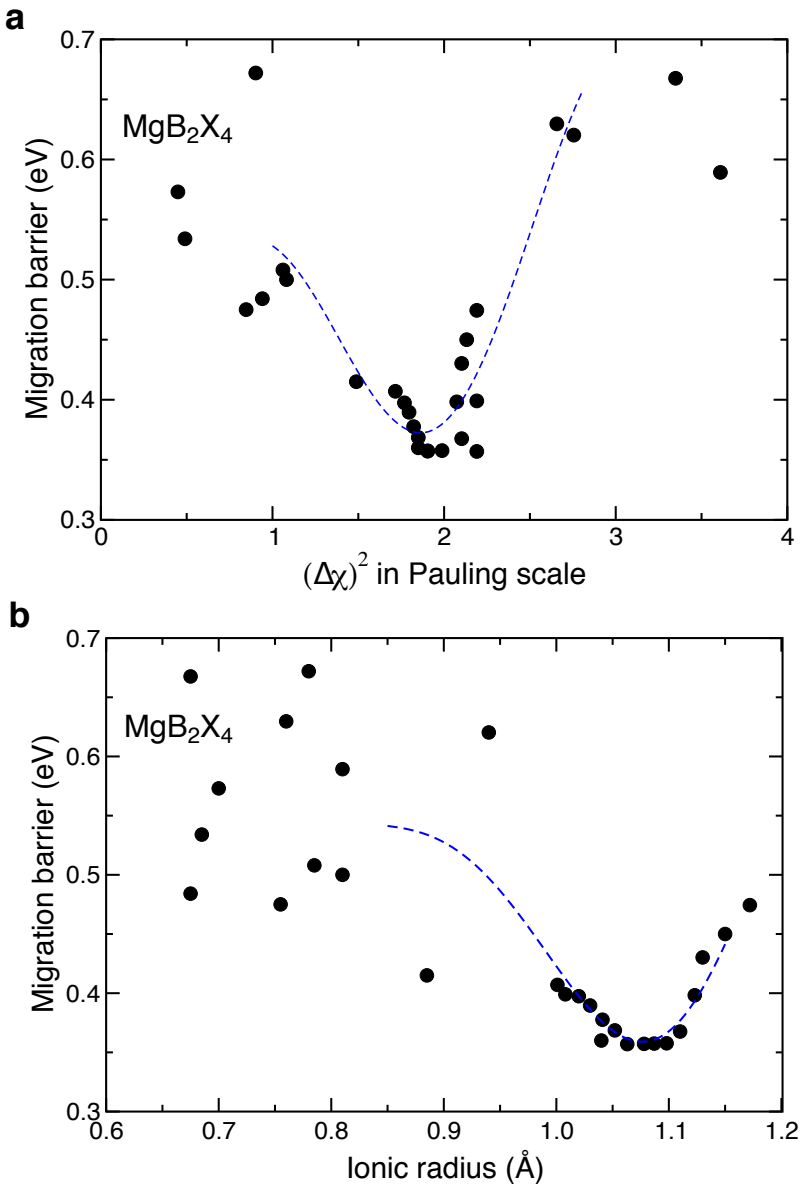

Figure 5: Mg migration barriers (in eV) as a function of the (a) squared electronegativity difference between transition metal B and anion X, and (b) the ionic radius of the transition metal B for a number of MgB_2X_4 spinels.

charge carriers A. Again a convincing linear scaling relation has been obtained.

The fact that the migration parameter $N_{\mathrm{migr}}^{\mathrm{AX}}$ captures the essence of the migration barrier height upon variation of the migrating cation A and the anion X of the host lattice calls for a critical assessment of this parameter. There are some obvious factors influencing the height of the migration barrier. For larger ions it will be harder to migrate through a given lattice,

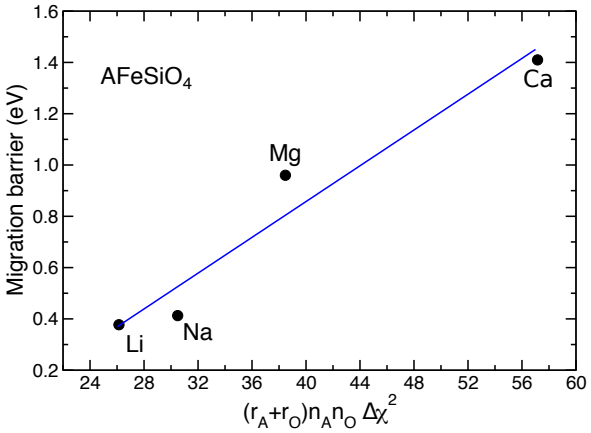

Figure 6: Migration barriers (in eV) in the olivine $AFeSiO_4$ as a function of the migration parameter $(r_A + r_X)n_A n_X \Delta\chi^2_{AX}$ (Eq. (2)) for varying charge carriers A.

therefore it is no surprise that the ion radius r_A enters the migration barrier. However, when also varying the size of the anion of the host lattice, it becomes apparent that it is both the size of the cation and of the anion represented by $r_A + r_X$ that is the critical length parameter, as already stressed in a previous study.[28] Furthermore, note that in many cases the dependence of the mobility on the ionic radius is not monotonic,[29] so any descriptor of the ion mobility taking into account the ionic radius needs to reflect this non-monotonic behavior.

It is also well-known that the charge of the migrating ion matters with respect to the ion mobility. The higher the charge of an ion, the stronger its interaction with the environment and thus the higher the migration barriers. This same argumentation of course also applies to the charge of the ions constituting the host lattice as the ionic interaction scales with the product of the charges of interacting ions. These charges enter the migration parameter through the product of the oxidation numbers $n_A n_X$.

However, it is important to realize that in the migration of "ions" in a host lattice it is not *a priori* clear that the "ions" keep their ionic charge. Any crystal containing migrating ions has to be overall charge neutral because macroscopically charged matter is unstable. Hence any charge on the migrating ions has to be compensated by the host lattice. Of course, the assumption that strong ions remain charged in a host lattice makes a lot of sense and is the

basis of the concept of formal oxidation numbers. Still, formal atomic charges in a material are no good observables because it can not be uniquely defined which electrons belong to the migration ion and which to the host lattice as the electrons are shared between the bonding partners. This is also the reason why there is a broad variety of different charge partition schemes[52–55] used in quantum chemical codes in order to derive atomic charge numbers which can give quite different quantitative results. And furthermore, there are hardly any chemical systems in which the interaction is either purely ionic or purely covalent or purely metallic. Therefore it is not surprising that trends in the ion mobility cannot be fully understood on the basis of formal oxidation states alone.

This deviation from the purely ionic interaction can be characterized by the difference in the electronegativity $\Delta\chi^2$ of the interacting compounds which is also the basis for the Van Arkel-Ketelaar triangle. In this context it should be noted that the Pauling electronegativity in the form revised by Allred[56] that has been used here is based on a quite accurate, semi-empirical formula for dissociation energies, namely

$$(\chi_{\mathrm{A}} - \chi_{\mathrm{B}})^2 = E_d(\mathrm{AB}) - \frac{E_d(\mathrm{AA}) + E_d(\mathrm{BB})}{2} \ . \tag{7}$$

This illustrates that the square of the difference in the electronegativities takes the deviation from a purely ionic interaction in a compound crystal into account. It is in fact true that the stronger polarizability of "soft" anions has already been used to explain the higher ion mobility in chalcogenides containing sulfur and selenide compared to oxides[13] with their softness reflected in the lower electronegativity of sulfur and selenide.[57,58] Still this notion had not been transferred into any descriptor concept before.

The fact that the migration parameter including $\Delta\chi^2$ yields such a good descriptor for the height of the migration barriers reconfirms that a purely ionic consideration of ion mobility in crystals does not capture all factors determining this mobility. It also means that this deviation from ionicity is the reason for the observed non-monotonic behavior of the

migration barriers as a function of the ionic radii which is correctly taken into account by including the factor $\Delta\chi^2$ in the migration parameter. It is also important to stress the fact that the parameters entering the migration number are basically independent of the particular structure of the considered host lattice, as they correspond to general atomic and ionic properties of the particular elements. The same parameters enter the scaling relations for binaries, spinels and olivines, confirming the general fundamental nature of the scaling relations.

Note that the linear scaling relations as a function of the migration parameter established in our work do not allow the quantitative prediction of the height of migration barriers in any particular system without any initially measured or calculated data. Thus they do not correspond to a parameterization of the barrier height as a function of input parameter across all families of possible structures. However, these scaling relations allow to make qualitative predictions of the height of migration barriers, and once some migration barriers are known in these structures, then even semi-quantitative predictions based on easily accessible materials parameters can be made. This will be very beneficial for the identification of promising candidate materials with improved mobility properties. Of course, this linear scaling is not perfect, and we already identified some outliers. However, this descriptor is based on a strict physico-chemical reasoning, so deviations from the scaling relations should point to some interesting additional factors also influencing the ion mobility and thus to an enhanced fundamental understanding of ion mobility.

Conclusions and Summary

In summary, we propose a descriptor called migration parameter for the ion mobility in crystalline solids that is based on well-accessible materials parameters, namely ion sizes, oxidation states and the Pauling electronegativity difference between anions and cations in the compounds. Thus in contrast to previous attempts to derive descriptors for the ion

mobility we also take the deviation from ionic bonding in the compounds into account. For a broad range of materials classes, we have shown that the height of the migration barrier follows linear scaling relations as a function of this descriptor upon both the variation of the cation chemistry of the migrating ion as well as upon variation of the anion chemistry of the host lattice. This demonstrates the strong predictive power of the descriptor which should accelerate the discovery of materials with improved migration properties in electrochemical energy storage and conversion.

Supporting Information - Computational details

DFT calculations

All first-principles calculations were performed in the framework of density-functional theory (DFT)[59,60] employing the Projector Augmented Wave (PAW)[46] method as implemented in the Vienna *Ab-initio* Simulation Package.[45,61,62] The exchange-correlation effects were described by the generalized gradient approximation (GGA) using the Perdew-Burke-Ernzerhof (PBE) functional.[47] The calculations were optimized using 2×2×2 k-point mesh, with a plane wave cutoff of 520 eV, and a convergency within 1×10^{-5} eV per supercell.

The nudged elastic band (NEB)[44,63] method is applied in the low vacancy limit to define ion migration barriers. This means that one cation vacancy was created in a large supercell to ensure the removal of defect-defect interactions across periodic boundaries in all cases, and the minimum energy path for the propagation of a neighboring cation into this vacancy was determined by the NEB calculations. All of the structures were fully relaxed until the forces on the atoms were converged within 0.05 eV $Å^{-1}$. The NEB calculations have been carried out with seven distinct images for binary compounds, and four distinct images for ternary spinels to evaluate the Mg-ion migration trajectory. Note that the diffusion in considered compounds is referred to interstitial diffusion in the literature.

Machine-learning approach

The compressed-sensing approach, developed by Ouyang et al.,[50] was performed based on the DFT-calculated data for accurate physical descriptor findings in the classification of the migration barriers. We have used the following input parameters to describe the migration barrier energy of binary compounds and ternary spinels: the stoichiometric number of elements, the electronegativity of each element, the atomic masses of elements, the ionic radii of elements, the valence electron numbers of each element, and the unit-cell volumes. Furthermore, the machine-learning process was operated within the scikit-learn package[64] using the Anaconda Distribution (Python 3.7.3, numpy 1.16.2).[65,66] The random forest algorithm[67] was employed for the data training and prediction and both regression and classification. The output includes the migration barrier energies of compounds. The effect of B cation in AB_2X_4 spinel was then calculated after obtaining these results. The machine-learning algorithm was verified by analyzing the mean absolute error (MAE).

Acknowledgments

Useful discussions with Jürgen Janek, University of Gießen, and Holger Euchner, Helmholtz-Institute Ulm, are gratefully acknowledged. This work contributes to the research performed at CELEST (Center for Electrochemical Energy Storage Ulm-Karlsruhe) and was funded by the German Research Foundation (DFG) under Project ID 390874152 (POLiS Cluster of Excellence). Further support by the Dr. Barbara Mez-Starck Foundation and computer time provided by the state of Baden-Württemberg through bwHPC and the German Research Foundation (DFG) through grant no INST 40/575-1 FUGG (JUSTUS 2 cluster) are gratefully acknowledged.

References

[1] Choi, S.; Wang, G. Advanced Lithium-Ion Batteries for Practical Applications: Technology, Development, and Future Perspectives. *Adv. Mater. Technol.* **2018**, *3*, 1700376.

[2] Ma, Y.; Ma, Y.; Giuli, G.; Euchner, H.; Groß, A.; Lepore, G. O.; d'Acapito, F.; Geiger, D.; Biskupek, J.; Kaiser, U. et al. Introducing Highly Redox-Active Atomic Centers into Insertion-Type Electrodes for Lithium-Ion Batteries. *Adv. Energy Mater.* **2020**, *10*, 2000783.

[3] Arroyo-de Dompablo, M. E.; Ponrouch, A.; Johansson, P.; Palacín, M. R. Achievements, Challenges, and Prospects of Calcium Batteries. *Chem. Rev.* **2020**, *120*, 6331–6357.

[4] Rajagopalan, R.; Tang, Y.; Ji, X.; Jia, C.; Wang, H. Advancements and Challenges in Potassium Ion Batteries: A Comprehensive Review. *Adv. Funct. Mater.* **2020**, *30*, 1909486.

[5] Elia, G. A.; Marquardt, K.; Hoeppner, K.; Fantini, S.; Lin, R.; Knipping, E.; Peters, W.; Drillet, J.-F.; Passerini, S.; Hahn, R. An Overview and Future Perspectives of Aluminum Batteries. *Adv. Mater.* **2016**, *28*, 7564–7579.

[6] Anji Reddy, M.; Helen, M.; Groß, A.; Fichtner, M.; Euchner, H. Insight into Sodium Insertion and the Storage Mechanism in Hard Carbon. *ACS Energy Lett.* **2018**, *3*, 2851–2857.

[7] Hwang, J.-Y.; Myung, S.-T.; Sun, Y.-K. Sodium-ion batteries: present and future. *Chem. Soc. Rev.* **2017**, *46*, 3529–3614.

[8] Yabuuchi, N.; Kubota, K.; Dahbi, M.; Komaba, S. Research Development on Sodium-Ion Batteries. *Chem. Rev.* **2014**, *114*, 11636–11682.

[9] Gregory, T. D.; Hoffman, R. J.; Winterton, R. C. Nonaqueous Electrochemistry of Magnesium: Applications to Energy Storage. *J. Electrochem. Soc.* **1990**, *137*, 775–780.

[10] Aurbach, D.; Lu, Z.; Schechter, A.; Gofer, Y.; Gizbar, H.; Turgeman, R.; Cohen, Y.; Moshkovich, M.; Levi, E. Prototype systems for rechargeable magnesium batteries. *Nature* **2000**, *407*, 724–727.

[11] MacLaughlin, C. M. Status and Outlook for Magnesium Battery Technologies: A Conversation with Stan Whittingham and Sarbajit Banerjee. *ACS Energy Lett.* **2019**, *4*, 572–575.

[12] Davidson, R.; Verma, A.; Santos, D.; Hao, F.; Fincher, C. D.; Zhao, D.; Attari, V.; Schofield, P.; Van Buskirk, J.; Fraticelli-Cartagena, A. et al. Mapping mechanisms and growth regimes of magnesium electrodeposition at high current densities. *Mater. Horiz.* **2020**, *7*, 843–854.

[13] Maroni, F.; Dongmo, S.; Gauckler, C.; Marinaro, M.; Wolfahrt-Mehrens, M. Through the Maze of Multivalent-ion Batteries: A Critical Review on the status of the research on cathode materials for Mg^{2+} and Ca^{2+} ions insertion. *Batteries & Supercaps* **2021**,

[14] Singh, N.; Arthur, T. S.; Ling, C.; Matsui, M.; Mizuno, F. A high energy-density tin anode for rechargeable magnesium-ion batteries. *Chem. Commun.* **2013**, *49*, 149–151.

[15] Zhao-Karger, Z.; Gil Bardaji, M. E.; Fuhr, O.; Fichtner, M. A new class of non-corrosive, highly efficient electrolytes for rechargeable magnesium batteries. *J. Mater. Chem. A* **2017**, *5*, 10815–10820.

[16] Aurbach, D.; Cohen, Y.; Moshkovich, M. The Study of Reversible Magnesium Deposition by In Situ Scanning Tunneling Microscopy. *Electrochem. Solid-State Lett.* **2001**, *4*, A113.

[17] Matsui, M. Study on electrochemically deposited Mg metal. *J. Power Sources* **2011**, *196*, 7048 – 7055.

[18] Zhao, Q. S.; Wang, J. L. Reversibility of electrochemical magnesium deposition from

tetrahydrofuran solutions containing pyrrolidinyl magnesium halide. *Electrochim. Acta* **2011**, *56*, 6530.

[19] Jäckle, M.; Groß, A. Microscopic properties of lithium, sodium, and magnesium battery anode materials related to possible dendrite growth. *J. Chem. Phys.* **2014**, *141*, 174710.

[20] Jäckle, M.; Helmbrecht, K.; Smits, M.; Stottmeister, D.; Groß, A. Self-diffusion barriers: Possible descriptors for dendrite growth in batteries? *Energy Environ. Sci.* **2018**, *11*, 3400–3407.

[21] Janek, J.; Zeier, W. G. A solid future for battery development. *Nature Energy* **2016**, *1*, 16141.

[22] Ikeda, S.; Takahashi, M.; Ishikawa, J.; Ito, K. Solid electrolytes with multivalent cation conduction. 1. Conducting species in Mg-Zr-PO_4 system. *Solid State Ionics* **1987**, *23*, 125 – 129.

[23] Halim, Z.; Adnan, S.; Mohamed, N. Effect of sintering temperature on the structural, electrical and electrochemical properties of novel $Mg_{0.5}Si_2(PO_4)_3$ ceramic electrolytes. *Ceram. Int.* **2016**, *42*, 4452 – 4461.

[24] Mohtadi, R.; Matsui, M.; Arthur, T. S.; Hwang, S.-J. Magnesium Borohydride: From Hydrogen Storage to Magnesium Battery. *Angew. Chem. Int. Ed.* **2012**, *51*, 9780–9783.

[25] Unemoto, A.; Matsuo, M.; Orimo, S.-i. Complex Hydrides for Electrochemical Energy Storage. *Adv. Funct. Mater.* **2014**, *24*, 2267–2279.

[26] Higashi, S.; Miwa, K.; Aoki, M.; Takechi, K. A novel inorganic solid state ion conductor for rechargeable Mg batteries. *Chem. Commun.* **2014**, *50*, 1320–1322.

[27] Canepa, P.; Bo, S.-H.; Sai Gautam, G.; Key, B.; Richards, W. D.; Shi, T.; Tian, Y.; Wang, Y.; Li, J.; Ceder, G. High magnesium mobility in ternary spinel chalcogenides. *Nat. Commun.* **2017**, *8*, 1759.

[28] Dillenz, M.; Sotoudeh, M.; Euchner, H.; Groß, A. Screening of Charge Carrier Migration in the $MgSc_2Se_4$ Spinel Structure. *Front. Energy Res.* **2020**, *8*, 260.

[29] Bachman, J. C.; Muy, S.; Grimaud, A.; Chang, H.-H.; Pour, N.; Lux, S. F.; Paschos, O.; Maglia, F.; Lupart, S.; Lamp, P. et al. Inorganic Solid-State Electrolytes for Lithium Batteries: Mechanisms and Properties Governing Ion Conduction. *Chem. Rev.* **2016**, *116*, 140–162.

[30] Rong, Z.; Malik, R.; Canepa, P.; Sai Gautam, G.; Liu, M.; Jain, A.; Persson, K.; Ceder, G. Materials Design Rules for Multivalent Ion Mobility in Intercalation Structures. *Chem. Mater.* **2015**, *27*, 6016–6021.

[31] Euchner, H.; Chang, J. H.; Groß, A. On stability and kinetics of Li-rich transition metal oxides and oxyfluorides. *J. Mater. Chem. A* **2020**, *8*, 7956–7967.

[32] Levi, E.; Gofer, Y.; Aurbach, D. On the Way to Rechargeable Mg Batteries: The Challenge of New Cathode Materials. *Chem. Mater.* **2010**, *22*, 860–868.

[33] Huie, M. M.; Bock, D. C.; Takeuchi, E. S.; Marschilok, A. C.; Takeuchi, K. J. Cathode materials for magnesium and magnesium-ion based batteries. *Coord. Chem. Rev.* **2015**, *287*, 15 – 27.

[34] Verma, V.; Kumar, S.; Manalastas Jr., W.; Satish, R.; Srinivasan, M. Progress in Rechargeable Aqueous Zinc- and Aluminum-Ion Battery Electrodes: Challenges and Outlook. *Adv. Sustainable Syst.* **2019**, *3*, 1800111.

[35] Yang, T.-Y.; Gregori, G.; Pellet, N.; Grätzel, M.; Maier, J. The Significance of Ion Conduction in a Hybrid Organic–Inorganic Lead-Iodide-Based Perovskite Photosensitizer. *Angew. Chem. Int. Ed.* **2015**, *54*, 7905–7910.

[36] Ghiringhelli, L. M.; Vybiral, J.; Levchenko, S. V.; Draxl, C.; Scheffler, M. Big Data of Materials Science: Critical Role of the Descriptor. *Phys. Rev. Lett.* **2015**, *114*, 105503.

[37] Isayev, O.; Oses, C.; Toher, C.; Gossett, E.; Curtarolo, S.; Tropsha, A. Universal fragment descriptors for predicting properties of inorganic crystals. *Nat. Commun.* **2017**, *8*, 15679.

[38] Nørskov, J. K.; Rossmeisl, J.; Logadottir, A.; Lindqvist, L.; Kitchin, J. R.; Bligaard, T.; Jónsson, H. Origin of the Overpotential for Oxygen Reduction at a Fuel-Cell Cathode. *J. Phys. Chem. B* **2004**, *108*, 17886–17892.

[39] Man, I. C.; Su, H.-Y.; Calle-Vallejo, F.; Hansen, H. A.; Martinez, J. I.; Inoglu, N. G.; Kitchin, J.; Jaramillo, T. F.; Nørskov, J. K.; Rossmeisl, J. Universality in Oxygen Evolution Electrocatalysis on Oxide Surfaces. *ChemCatChem* **2011**, *3*, 1159–1165.

[40] Wang, Y.; Richards, W. D.; Ong, S. P.; Miara, L. J.; Kim, J. C.; Mo, Y.; Ceder, G. Design principles for solid-state lithium superionic conductors. *Nat. Mater.* **2015**, *14*, 1026.

[41] Muy, S.; Bachman, J. C.; Giordano, L.; Chang, H.-H.; Abernathy, D. L.; Bansal, D.; Delaire, O.; Hori, S.; Kanno, R.; Maglia, F. et al. Tuning mobility and stability of lithium ion conductors based on lattice dynamics. *Energy Environ. Sci.* **2018**, *11*, 850–859.

[42] Gordiz, K.; Muy, S.; Zeier, W. G.; Shao-Horn, Y.; Henry, A. Enhancement of ion diffusion by targeted phonon excitation. *Cell Reports Physical Science* **2021**, *2*, 100431.

[43] Henß, A.-K.; Sakong, S.; Messer, P. K.; Wiechers, J.; Schuster, R.; Lamb, D. C.; Groß, A.; Wintterlin, J. Density fluctuations as door-opener for diffusion on crowded surfaces. *Science* **2019**, *363*, 715–718.

[44] Henkelman, G.; Jónsson, H. Improved tangent estimate in the nudged elastic band method for finding minimum energy paths and saddle points. *J. Chem. Phys.* **2000**, *113*, 9978.

[45] Kresse, G.; Furthmüller, J. Efficient iterative schemes for ab initio total-energy calculations using a plane-wave basis set. *Phys. Rev. B* **1996**, *54*, 11169–11186.

[46] Blöchl, P. E. Projector augmented-wave method. *Phys. Rev. B* **1994**, *50*, 17953–17979.

[47] Perdew, J. P.; Burke, K.; Ernzerhof, M. Generalized Gradient Approximation Made Simple. *Phys. Rev. Lett.* **1996**, *77*, 3865–3868.

[48] Sotoudeh, M.; Dillenz, M.; Groß, A. Mechanism of magnesium transport in spinel chalcogenides. *Preprint* **2021**, https://doi.org/10.21203/rs.3.rs–358467/v2.

[49] Allen, L. C.; Capitani, J. F.; Kolks, G. A.; Sproul, G. D. Van Arkel—Ketelaar triangles. *J. Mol. Struct.* **1993**, *300*, 647–655.

[50] Ouyang, R.; Curtarolo, S.; Ahmetcik, E.; Scheffler, M.; Ghiringhelli, L. M. SISSO: A compressed-sensing method for identifying the best low-dimensional descriptor in an immensity of offered candidates. *Phys. Rev. Materials* **2018**, *2*, 083802.

[51] Hörmann, N.; Groß, A. Stability, composition and properties of Li_2FeSiO_4 surfaces studied by DFT. *J. Solid State Electrochem.* **2014**, *18*, 1401–1413.

[52] Yu, M.; Trinkle, D. R. Accurate and efficient algorithm for Bader charge integration. *J. Chem. Phys.* **2011**, *134*, 064111.

[53] Tang, W.; Sanville, E.; Henkelman, G. A grid-based Bader analysis algorithm without lattice bias. *J. Phys.: Condens. Matter* **2009**, *21*, 084204.

[54] Wiberg, K. B.; Rablen, P. R. Comparison of atomic charges derived via different procedures. *J. Comput. Chem.* **1993**, *14*, 1504–1518.

[55] De Proft, F.; Van Alsenoy, C.; Peeters, A.; Langenaeker, W.; Geerlings, P. Atomic charges, dipole moments, and Fukui functions using the Hirshfeld partitioning of the electron density. *J. Comput. Chem.* **2002**, *23*, 1198–1209.

[56] Allred, A. Electronegativity values from thermochemical data. *J. Inorg. Nucl. Chem.* **1961**, *17*, 215 – 221.

[57] Liu, M.; Jain, A.; Rong, Z.; Qu, X.; Canepa, P.; Malik, R.; Ceder, G.; Persson, K. A. Evaluation of sulfur spinel compounds for multivalent battery cathode applications. *Energy Environ. Sci.* **2016**, *9*, 3201–3209.

[58] Mao, M.; Ji, X.; Hou, S.; Gao, T.; Wang, F.; Chen, L.; Fan, X.; Chen, J.; Ma, J.; Wang, C. Tuning Anionic Chemistry To Improve Kinetics of Mg Intercalation. *Chem. Mater.* **2019**, *31*, 3183–3191.

[59] Hohenberg, P.; Kohn, W. Inhomogeneous Electron Gas. *Phys. Rev.* **1964**, *136*, B864–B871.

[60] Kohn, W.; Sham, L. J. Self-Consistent Equations Including Exchange and Correlation Effects. *Phys. Rev.* **1965**, *140*, A1133–A1138.

[61] Kresse, G.; Hafner, J. Ab initio molecular dynamics for liquid metals. *Phys. Rev. B* **1993**, *47*, 558–561.

[62] Kresse, G.; Joubert, D. From ultrasoft pseudopotentials to the projector augmented-wave method. *Phys. Rev. B* **1999**, *59*, 1758–1775.

[63] Sheppard, D.; Terrell, R.; Henkelman, G. Optimization methods for finding minimum energy paths. *J. Chem. Phys.* **2008**, *128*, 134106.

[64] Pedregosa, F.; Varoquaux, G.; Gramfort, A.; Michel, V.; Thirion, B.; Grisel, O.; Blondel, M.; Prettenhofer, P.; Weiss, R.; Dubourg, V. et al. Scikit-learn: Machine Learning in Python. *J. Mach. Learn. Res.* **2011**, *12*, 2825–2830.

[65] Harris, C. R.; Millman, K. J.; van der Walt, S. J.; Gommers, R.; Virtanen, P.; Cournapeau, D.; Wieser, E.; Taylor, J.; Berg, S.; Smith, N. J. et al. Array programming with NumPy. *Nature* **2020**, *585*, 357–362.

[66] Kluyver, T.; Ragan-Kelley, B.; Pérez, F.; Granger, B.; Bussonnier, M.; Frederic, J.; Kelley, K.; Hamrick, J.; Grout, J.; Corlay, S. et al. In *Positioning and Power in Academic*

Publishing: Players, Agents and Agendas; Loizides, F., Schmidt, B., Eds.; 2016; pp 87 – 90.

[67] Liaw, A.; Wiener, M. Classification and Regression by randomForest. *R News* **2002**, *2*, 18–22.